Isolating the contributions of specific network sites to the diffuse vibrational spectrum of interfacial water with isotopomer-selective spectroscopy of cold clusters

Journal:	*The Journal of Physical Chemistry*
Manuscript ID	Draft
Manuscript Type:	Feature Article
Date Submitted by the Author:	n/a
Complete List of Authors:	Yang, Nan; Yale University Department of Chemistry, Khuu, Thien; Yale University, Chemistry Mitra, Sayoni; Yale University Duong, Chinh; Yale University, Chemistry Johnson, Mark; Yale University, Chemistry DiRisio, Ryan; University of Washington McCoy, Anne; University of Washington, Department of Chemistry Miliordos, Evangelos; Auburn University, Chemistry and Biochemistry Xantheas, Sotiris; Pacific Northwest National Laboratory, Advanced Computing, Mathamatics and Data

Isolating the contributions of specific network sites to the diffuse vibrational spectrum of interfacial water with isotopomer-selective spectroscopy of cold clusters

Nan Yang,[a] Thien Khuu,[a] Sayoni Mitra,[a] Chinh H. Duong,[a] and Mark A. Johnson[a,*]

Ryan J. DiRisio[b] and Anne B. McCoy[b]

Evangelos Miliordos[c,1] and Sotiris S. Xantheas[b,c]

[a] Sterling Chemistry Laboratory, Yale University, New Haven, CT, 06520

[b] Department of Chemistry, University of Washington, Seattle, WA 98195, USA

[c] Advanced Computing, Mathematics and Data Division, Pacific Northwest National Laboratory, 902 Battelle Boulevard, P.O. Box 999, MS K1-83, WA, 99352

Mark A. Johnson Email: mark.johnson@yale.edu

Anne B. McCoy Email: abmccoy@uw.edu

Sotiris S. Xantheas Email: sotiris.xantheas@pnnl.gov and xantheas@uw.edu

[1] Present address: Department of Chemistry and Biochemistry, Auburn University, Auburn, AL 36849-5312

Abstract:

Decoding the structural information contained in the interfacial vibrational spectrum of water requires understanding how the spectral signatures of individual water molecules respond to their local hydrogen bonding environments. In this study, we isolated the contributions for the five classes of sites that differ according to the number of donor (D) and acceptor (A) hydrogen bonds that characterize each site. These patterns were measured by exploiting the unique properties of the water cluster cage structures formed in the gas phase upon hydration of a series of cations $M^+\cdot(H_2O)_n$ (M=Li, Na, Cs, NH_4, CH_3NH_3, H_3O, and n=5, 20-22). This selection of ions was chosen to systematically express the A, AD, AAD, ADD, and AADD hydrogen bonding motifs. The spectral signatures of each site were measured using two-color, IR-IR isotopomer-selective photofragmentation vibrational spectroscopy of the cryogenically cooled, mass selected clusters ions in which a single intact H_2O is introduced without isotopic scrambling, an important advantage afforded by the cluster regime. The resulting patterns provide an unprecedented picture of the intrinsic lineshapes and spectral complexities associated with excitation of the individual OH groups, as well as the correlation between the frequencies of the two OH groups on the same water molecule, as a function of network site. The properties of the surrounding water network that govern this frequency map are evaluated by dissecting electronic structure calculations that explore how changes in the nearby network structures, both within and beyond the first hydration shell, affect the local frequency of an OH oscillator. The qualitative trends are recovered with a simple model that correlates the OH frequency with the network-modulated local electron density in the center of the OH bond.

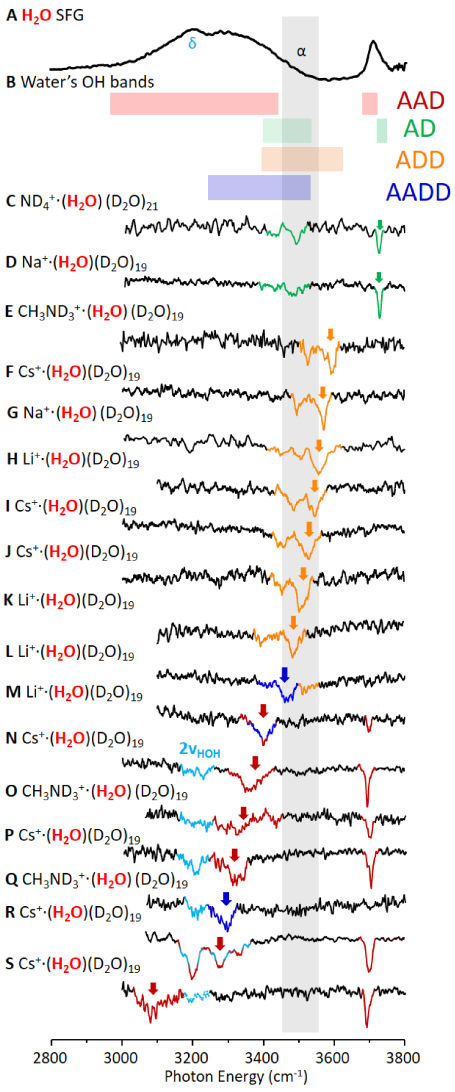

I. Introduction

The very large range (3000-3700 cm^{-1}) spanned by the OH stretching vibrational spectrum of liquid water reveals the wide distribution of intramolecular distortions caused by variations in the H-bonding topologies of the surrounding network. The distribution of OH frequencies has been considered in the context of the local electric fields that are present in particular binding sites, which in turn reflect the number of directly coordinated water molecules as well as the orientations of water molecules in the more distant hydration shells.[1-4] The variation in this coordination number is particularly relevant to the spectrum of the air-water interface, where there are many non-bonded OH groups. There is a consensus that the dominant interactions governing the local OH frequency are the number of H-bond donor (D) and acceptor (A) molecules attached to the water molecule in question.[3-5] The OH frequency distributions reported by Skinner and coworkers[1, 4] for five classes of coordination environment (A, AD, AAD, ADD, and AADD) are reproduced in Fig. 1 to illustrate the ranges of activity expected for each class.[4] Note that within a coordination class, the distributions are very broad such that the red-shifted bands arising from the bound OH groups overlap, as do the fundamentals arising from the non-bonded OH groups near 3700 cm^{-1}. As such, the factors that govern the local frequency must reflect different topologies of the water network beyond the first shell. Consequently, both Skinner[5] and Ohno[3] have advanced more elaborate schemes that take into account the coordination environments of the water molecules that are attached to the molecule whose frequency is under consideration. Although the simulations provide a compelling microscopic picture of how different structures contribute to the spectrum, experimental verification of these predicted contributions presents a profound challenge. For example, recent efforts to directly extract the contribution from the 3500 cm^{-1} region using surface-sensitive spectroscopies yielded different spectral responses, pointing to the complexities of isolating the ambient (as opposed to laser-driven) contributions to the linear spectrum.[6-7]

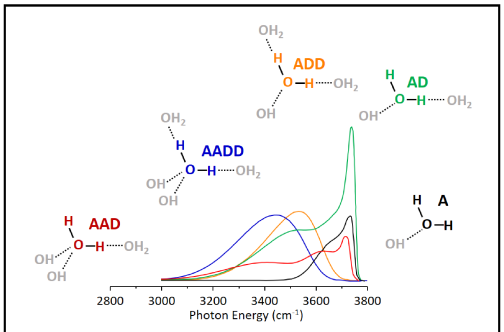

Figure 1. Color-coded frequency distributions of the two OH stretches arising from water molecules surrounded by various acceptor (A) and donor (D) H-bonding arrangements. Reproduced from Ni et al. (ref.4) with permission.

Very recently, the unique advantages of cryogenic, gas phase cluster spectroscopy[8-9] have proven useful to disentangle the contributions of the AAD and ADD sites using the $Cs^+\cdot(H_2O)_{20}$ cluster as a model system.[10] This system adopts a clathrate cage structure constructed from 12 interlocking, cyclic water pentamers (a pentagonal dodecahedron, PD). The advantage of the PD structure is that it only has 10 AAD and ADD sites, thus eliminating congestion from other sites. Importantly, the OH stretching spectrum of $Cs^+\cdot(H_2O)_{20}$ is still diffuse, spanning the range displayed by the air-water interface (see Fig. 2E). This occurs despite the fact that only two sites are in play because the surrounding network topologies are quite diverse with respect to the H-bond configurations in the surrounding hydration shells, with the result that the bound OH (hereafter OH^b) contributions occur over hundreds of wavenumbers. Nonetheless, these overlapping contributions could be completely disentangled by leveraging cluster regime suppression of H/D isotopic exchange.[11-12] This allows the incorporation of a single, intact H_2O molecule into an otherwise perdeuterated water cage. The labeled water was observed to statistically occupy all spectroscopically distinct sites, creating an isotopologue that is a heterogeneous ensemble of isotopomers that differ according to the site occupied by the isotopic label. The vibrational spectrum of each isotopomer can then be isolated experimentally using two-color, IR-IR photobleaching techniques routinely used in ion photodissociation spectroscopy to separate the spectra of structural isomers.[8]

Importantly, because there is only one H_2O molecule in any given cluster, the spectrum of each isotopomer consists of the *correlated absorptions of its two OH groups and any "extra" features arising from anharmicities*.[8, 13] We herein present the results of similar site-specific measurements on a series of water clusters where both cluster size and guest cation are varied systematically to reveal the spectral signatures of all the sites that are relevant to the deconstruction of the interfacial IR spectrum. The particular systems selected to accomplish this goal are indicated in Fig. 2C-G along with their vibrational spectra obtained by IR photodissociation of a weakly bound D_2 molecule. The sum of these spectra (Fig. 2B) is compared to the surface-selective (sum frequency generation, SFG) spectrum of the water interface[14-16] (Fig. 2A) to confirm that, taken together, the cluster systems span the same frequency range. Note that the selection rules for SFG are different than those of the linear absorption regime at play in the cluster spectra and differences in shape are expected.[1, 4] We consider the site-specific contributions to this broad envelope in the context of qualitative rules of H-bonding commonly invoked to deconstruct the spectrum of the air-water interface.

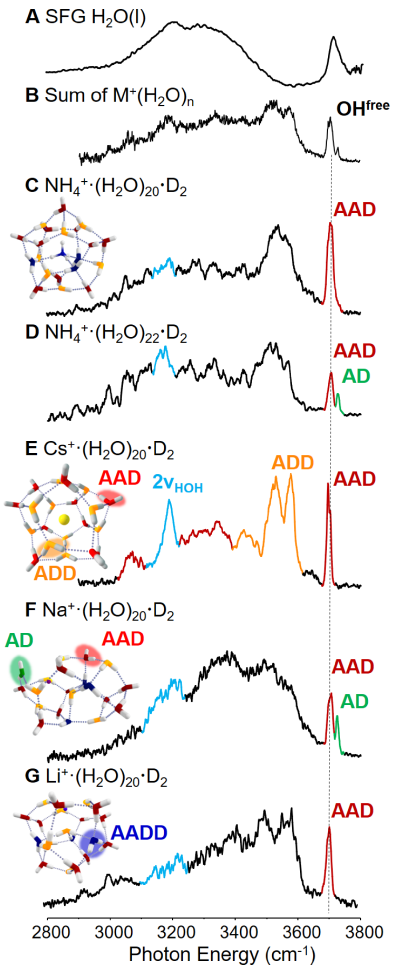

Figure 2. SFG spectrum of the air water interface compared to the spectra of various water clusters in the OH region. (A) SFG intensity ($|\chi^{(2)}|^2$) spectrum reproduced from ref.15 with permission; δ denotes the bend overtone ($2\nu_{HOH}$) transition and α denotes the controversial region around 3500 cm^{-1}. (B) Sum of cluster spectra in (C-G) weighted equally by peak area. D_2-tagged predissociation spectra and representative structures of (C) $NH_4^+\cdot(H_2O)_{20}$, (D) $NH_4^+\cdot(H_2O)_{22}$, (E) $Cs^+\cdot(H_2O)_{20}$, (F) $Na^+\cdot(H_2O)_{20}$, and (G) $Li^+\cdot(H_2O)_{20}$.[19] OH stretching bands and water molecules in the structures are color-coded according to their types.

II. Results and Discussion

II.A Dependence of water network structures and H-bonding site types on cation and size

The calculated structures for the cluster scaffolds used for this study are depicted in the inserts in Fig. 2C-G with the various sites highlighted in color. Rotatable pdf images are included in the SI. Note that the cluster structures in the n~20 size range adopt many thousands of isomeric forms that have similar oxygen atom frameworks, but differ according to the orientations and topologies of the H-bonds that connect them.[17] These isomers are close in energy and are undoubtedly present under our experimental conditions, hence providing a large variation in local H-bond environments that contributes to the signal at any given frequency. As such, the ensemble of ~10,000 ions interrogated in these measurements resembles the diverse environments experienced by interfacial water molecules in liquid or amorphous ice.

The changes in the cage structure with the size of the ion are reflected in the structures of the Li^+, Na^+, and Cs^+ clusters with 20 water molecules. The $Na^+\cdot(H_2O)_{20}$ structure (Fig. 2F) features a partial collapse of the PD cage present in the $Cs^+\cdot(H_2O)_{20}$ system (Fig. 2E) as the Na^+ ion migrates toward the surface, while the Li^+ ion is embedded onto the surface in $Li^+\cdot(H_2O)_{20}$ (Fig. 2G).[18-19] The

ammonium ion, on the other hand, resides in the center of the $(H_2O)_{20}$ cluster but puckers the cage due to strong, directional interactions between H_2O and NH_4^+ as indicated in Fig. 2C.[20] Table S1 presents a summary of the number of each site types are predicted for calculated structures of the various systems used in the this work.

The spectra in Fig. 2 illustrate how a specific H_2O bonding site can be introduced into the network by varying both ion identity and cluster size. For example, the distorted $Na^+\cdot(H_2O)_{20}$ system displays the telltale AD band (weaker member of the doublet in the OH^{free} stretching region highlighted in green), while the more symmetrical cage $Cs^+\cdot(H_2O)_{20}$ does not (compare Fig. 2E and 2F). Although the AD peak is missing in the $NH_4^+\cdot(H_2O)_{20}$ spectrum (Fig. 2C), it is present upon addition of two water molecules in the n=22 cluster (green shoulder in Fig. 2D). The spectral signatures of these AD binding sites can thus be isolated because the OH_{AD}^{free} band arising from this motif is clearly resolved between the free OH feature of the AAD molecules and the asymmetric stretch of water molecules in the A sites.[21] The latter are known from their positions in smaller cluster spectra with the sharp bands from $H_3O^+\cdot(H_2O)_5$ displayed in Fig. 4E, consistent with the simulated frequency distribution of this site on the interface in Fig.1 (black trace).[1, 22] We note that the absence of this OH_{AD}^{free} feature was key to the identification of the PD structures of $Cs^+\cdot(H_2O)_{20}$ and $H_3O^+\cdot(H_2O)_{20}$,[23-24] and the emergence of the AD feature in the $Cs^+\cdot(H_2O)_{20}$ spectrum at elevated temperature (200 K) has been recently exploited as a probe for the breakup of the PD cage.[25] On the other hand, isolation of the AADD site is the most challenging to achieve in the cluster systems because its features are expected to overlap with those from OH_{AAD}^{b}. (Fig. 1). The AADD sites are present in the n~20 range in systems that accommodate the ions on the surface of the cage. This is the case in the $H_3O^+\cdot(H_2O)_{20}$ structure, for example, which features 5 AADD sites.[26] Unfortunately, it is not possible to incorporate an intact H_2O molecule in the $D_3O^+\cdot(D_2O)_{20}$ structure due to fast H/D exchange, but the hydrophobic methyl group in the $CH_3NH_3^+$ ion also forces surface hydration in the $CH_3NH_3^+\cdot(H_2O)_{20}$ system. That system is also calculated to accommodate 5 molecules in AADD sites (see Table S1), but importantly does not exhibit H/D exchange because of the increased basicity of the amine group, and hence was chosen for this study. To gauge the extent of the spectral coverage afforded by our choice of cluster systems, Fig. 3 presents histograms of the calculated harmonic spectra, sorted and color coded by site type. We emphasize that this indicates the range of behaviors exhibited by specific structure types. It

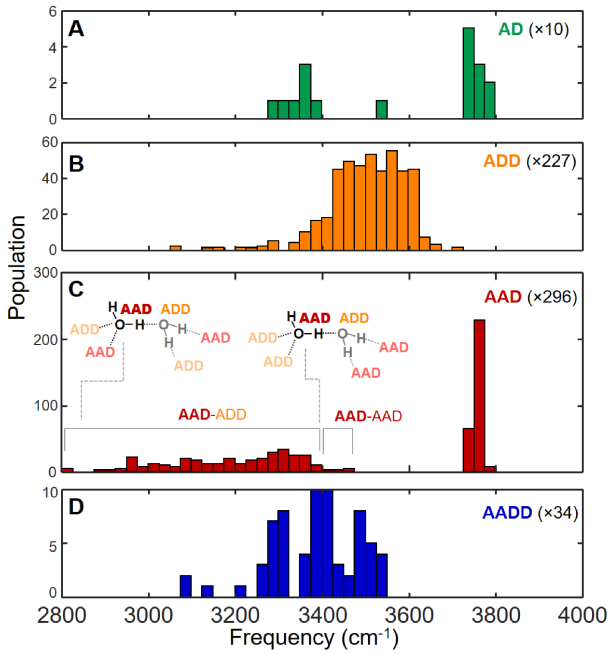

Figure 3. Calculated harmonic frequency distribution of various isomers of the $M^+\cdot(H_2O)(D_2O)_{n-1}$ (M=Li, Na, Cs, NH_4, CH_3NH_3, H_3O, and n=20-22) clusters. The calculations were done at B3LYP/6-31++G** level of theory and basis with the LANL2DZ pseudopotential for Cs and scaled by 0.973. The numbers near the A/D labels are the total number of water molecules shown in the panel. The bound OH in panel C are classified according to the binding site types of the OH group of interest and its surrounding water molecules.

is expected that many more isomers are generated in the ion source, and thus provide an even more complete sampling of the environments available to water molecules embedded in an extended network.

II.B. Survey of the site-dependent spectral patterns displayed by a single H_2O molecule embedded in three-dimensional H-bonded cages

Isotopomer-selective spectra were obtained using a two-color, IR-IR photobleaching variation in tandem photofragmentation mass spectrometry described in detail in ref. 8. Briefly, a particular isotopomer with composition $M^+ \cdot (H_2O)(D_2O)_n$ is mass selected for interaction with a probe laser with its frequency fixed on a transition associated with one of its isotopomers. The photofragment from the probe laser is monitored continuously to record the population in the isotopomer selected according to the carrier of the band to which it is tuned. Prior to this interaction, a powerful photobleaching laser intercepts the same ion packet and removes the population of each isotopomer as it is scanned across the entire spectrum. Hence all bands associated with the two OH groups on the site occupied by the single H_2O molecule then appear as downward going features (dips) according the population depletions driven by the bleach laser as it scanned across the spectrum.

Figure 4 presents a summary of a large data set collected using the six cations and various water cluster sizes, which were selected to illustrate the different (persistent) patterns associated with the various site types. The entire set is included in Fig. S1. These patterns were obtained by scanning the bleach laser while fixing a probe laser at the locations of the downward arrows. The most difficult site to reveal is the AADD because it does not have a unique spectral feature in the high energy region, and the samples presented in Fig. 4H required deconvolution as described in detail in section S.II of the SI.

An interesting feature of the patterns displayed in Fig. 4 is that they are quite simple, mostly consisting of two features as would be expected for the two OH stretching fundamentals on a water molecule at the harmonic level. The only exception is the "extra" band (turquoise in Fig. 4C and 4H) that appears around 3200 cm^{-1}. This feature arises from a Fermi-resonance interaction between the overtone of the HOH bending mode and OH stretching fundamentals that are red-shifted into resonance with the bend overtone.[10, 27] The simplicity of these patterns (compared to the complex spectra of the homogeneous isotopomers in Fig. 2) is important because it demonstrates that the spectral signatures of the embedded water molecules are not complicated by the presence of combination bands with soft modes. Such complications are known to arise from surprisingly strong electrical and mechanical anharmonicities in smaller water cluster ion systems.[8, 28-30] The widths of the bands, on the other hand, appear to systematically increase with red-shift, an effect noted earlier in the case of the isolated OH groups in spectra obtained by incorporation of a single HOD molecule in the 20 water molecule cages.[31]

The site-specific band patterns (Fig. 4) provide a remarkably clear picture of how the local H-bonding configuration drives the qualitative trends in the embedded band patterns (Fig. 2). We begin with the simple doublet pattern associated a single acceptor water molecule ('A' in Fig.1) attached to an OH group such that both of its OH groups are free (Fig. 4E). These two bands are the fundamentals of the symmetric (ν_{sym}) and antisymmetric (ν_{asym}) OH stretching normal modes, which lie very close to the origins of those found in the bare water molecule (gray downward arrows in Fig. 4E). If one adopts a local OH mode perspective, the ~100 cm^{-1} spacing between these bands can be viewed as the coupling

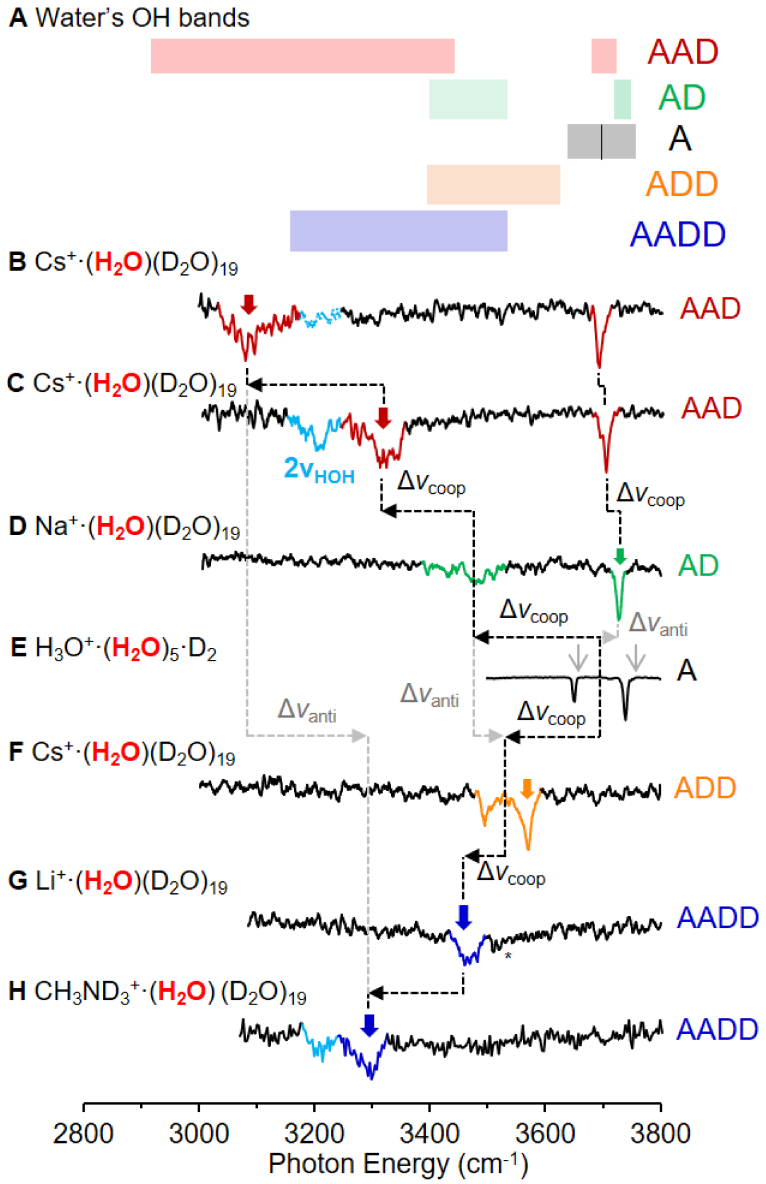

Figure 4. Frequency ranges of the various binding sites available to water molecules at the interface, with representive spectral patterns displayed by a single H_2O molecule embedded in each site. (A) Frequency ranges displayed by a single H_2O molecule embedded in D_2O clusters in various combinations of acceptor 'A' and donor 'D' H-bonding environments. (B-H) Representative patterns of the spectral signatures of the sites obtained from isotopomer-specific spectra of (B, C, F) $Cs^+\cdot(H_2O)(D_2O)_{19}$, (D) $Na^+\cdot(H_2O)(D_2O)_{19}$, (E) $H_3O^+\cdot(H_2O)_5$, (G) $Li^+\cdot(H_2O)(D_2O)_{19}$, and (H) $CH_3ND_3^+\cdot(H_2O)(D_2O)_{19}$. The OH stretching bands are color-coded according to their site types in (A). The complete set of spectra is included in Fig. S1. $2\nu_{HOH}$ denotes the bend overtone, while $\Delta\nu_{coop}$ and $\Delta\nu_{anti}$ labels on arrows denotes the frequency shifts caused by cooperative and anticooperative interactions displayed by adding a second H-bond to an open coordination site.

matrix element between the degenerate OH groups. Interestingly, when the A motif reorients into the surface to donate two H-bonds and adopt the ADD environment, the doublet pattern (Fig. 4F) retains the ~2/1 intensity ratio with about 20% contraction of the splitting while the centroid red-shifts by about 200 cm^{-1} ($\Delta\nu_{coop}$ in Fig. 4E, 4F). This red-shift is increased upon accepting another H-bond to form the AADD

(Fig. 4G and 4H), which is the behavior expected for cooperative H-bonding in which accepting a second H-bond enhances the first). Notice, however, that the broad OH^b_{AADD} feature does not appear as a doublet, suggesting that the second acceptor H-bond suppresses the coupling between the OH groups. Interestingly, Skinner and co-workers[32] considered this intramolecular coupling in simulations of condensed phase water and ice and concluded that the coupling matrix element is indeed reduced in the fully coordinated environment. Although the signal-to-noise in the AADD spectra is somewhat degraded, the trace in Fig. 4H suggests that the Fermi resonance with the bend overtone is retained, a provocative observation that warrants further investigation beyond the scope of this work.

The traces progressing upward from Fig. 4E display the trends associated with retention of one free OH group while donating an H-bond with its partner OH group, and sequentially adding acceptor groups. The formation of one donor bond to the A site creates the AD site (Fig. 4D), which results in a ~200 cm^{-1} red shift in the OH^b_{AD} stretch as expected. Note that the OH^{free}_{AD} band also red-shifts, and moves toward the 3705 cm^{-1} centroid of the normal modes in a free water molecule (the same frequency as the OH stretch in isolated HOD).[33] The latter shift occurs because the coupling between the two groups is suppressed when the separation between the two bands is significantly larger than the intrinsic coupling matrix element (~50 cm^{-1}). Although the red-shifted OH^b_{AD} fundamental is broadened (from 10 to 35 cm^{-1}) in keeping with expected H-bond behavior, it does not exhibit the intensity enhancement that is typical for H-bonds in binary systems.[34] When the AD site accepts another bond to form the AAD site, the OH^{free}_{ADD} transition falls closer to the decoupled OH stretch in HOD, and its companion OH^b_{AAD} transition further red-shifts by 200-400 cm^{-1} ($\Delta\nu_{coop}$ in Fig. 4C, D) as it broadens and gains intensity.

Finally, the survey in Fig. 4 also reveals the consequence of converting an AD site (Fig. 4D) into an ADD site (Fig. 4F) by forming a second donor bond. This blue shifts ν^b_{AD} by about 50 cm^{-1} ($\Delta\nu_{anti}$ between Fig. 4D and 4F) toward the centroid of the doublet in the OH^b_{ADD} pattern, indicating a weakening or anticooperative interaction between the two bound OH groups. A similar effect is observed in the case of transforming AAD into AADD (Fig. 4B and 4H).

II.C Frequency ranges explored by the A, AD, ADD and AAD sites

Figure 5 compares the frequency ranges associated with each binding class, which are displayed along with the predicted contributions to the spectrum of the air-water interface (solid curves above experimental spectra in Fig. 5). [1, 22]

The frequency range displayed by the A sites is readily available because the ν_{sym} and ν_{asym} bands are easily identified in the linear absorption spectrum. To sample the range available to the A sites, however, we note that these only occur in minimum energy structures at smaller cluster sizes. In general, the free OH frequency has been correlated with the local electric field at the surface,[34-36] such that the centroid of the ν_{sym} and ν_{asym} doublet red-shifts as the two bands come closer together. Several examples demonstrating this effect are included in Fig. 5A in which H_2O is attached to a water molecule, a hydronium ion, a proton, Mn^+ and Mn^{2+} (Fig. 5A2-A6, respectively)[35]. Note that the intensity of the two bands also inverts in a strong electric field such that the lower energy ν_{sym} band is dominant upon attachment to a +2 charged ion. The calculated range at the interface samples much of this range, but likely does so because of large amplitude dispacements driven by thermal fluctuations, which bring the nominally free OH groups closer to H-bond acceptors on the surface. Part of this effect can also be

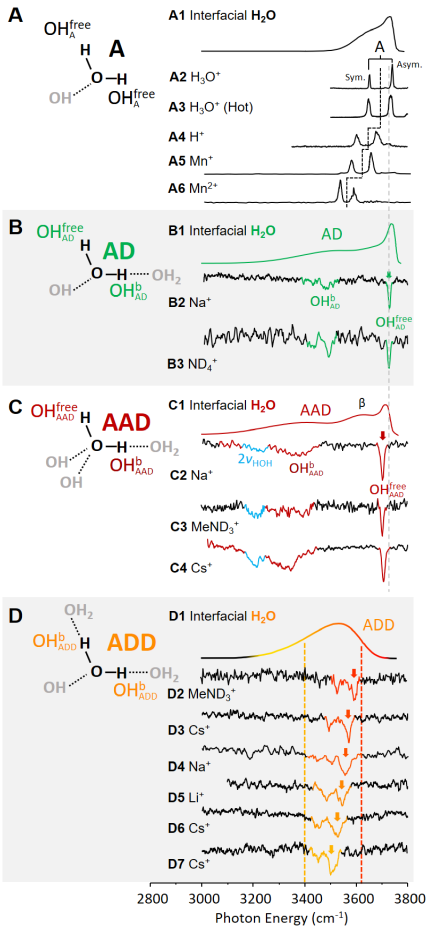

Figure 5. Calculated OH frequency distribution of water molecules classified by their H-bond environment at the air water interface compared to spectra obtained with finite size water clusters of the corresponding sites. Example structures, calculated frequency distributions (ref. 4, upward traces), and experimental spectra (downward traces) from various water clusters of single acceptor (A), acceptor-donor (B), acceptor-acceptor-donor (C) and acceptor-donor-donor (D) water molecules. The spectra are color coded according to the water molecule's acceptor donor type. Spectra from specific clusters are presented in (A2) $H_3O^+\cdot(H_2O)_5$, (A3) $H_3O^+\cdot(H_2O)_3$, (A4) $H^+\cdot(H_2O)_2$, (A5) $Mn^+\cdot(H_2O)$, (A6) $Mn^{2+}\cdot(H_2O)$, and (B3) $ND_4^+\cdot(H_2O)(D_2O)_{21}$. The rest have the M^+ labels correspond to the cation in a $M^+\cdot(H_2O)(D_2O)_{19}$, for example (B2) would be $Na^+\cdot(H_2O)(D_2O)_{19}$. (A5, A6) are reproduced from ref.35 with permission.

simulated using clusters warmed by absorption of a IR photon, leading to the broadened feature displayed in Fig. 5A3.

The frequency ranges explored by the **bound** OH^b_{AD} and OH^b_{AAD} oscillators can be unambiguously determined using IR^2MS^3 spectroscopy in a mode where the probe laser is tuned to one of the well-resolved **free** partner oscillators (OH^{free}_{AD} and OH^{free}_{AAD}), highlighted in green and red in Fig. 2, respectively. Specifically, by setting the probe laser on one of these bands, the locations of *all* of the absorptions arising from the bound OH groups within each class, OH^b_{AD} and OH^b_{AAD}, are revealed by scanning the bleach laser through the spectrum. The OH^b_{AD} bands were obtained by applying the IR^2MS^3 method to the $ND_4^+\cdot(H_2O)(D_2O)_{21}$ and $Na^+\cdot(H_2O)(D_2O)_{19}$ clusters. Both systems yield OH^b_{AD} activity over a narrow (~100 cm^{-1}) range near 3500 cm^{-1}, consistent with the simulated contributions from AD molecules displayed in Fig. 5B1.

In contrast to the AD behavior, the OH^b_{AAD} contributions span a larger range from 3100 to 3450 cm^{-1}. Note that the $Na^+\cdot(H_2O)(D_2O)_{19}$ system exhibits both AAD and AD sites so that the different behaviors are displayed by the same cluster. In addition, the range of its OH^b_{AAD} envelope, as well as that displayed by $CH_3ND_3^+\cdot(H_2O)(D_2O)_{19}$, are similar to that found in the more symmetrical $Cs^+\cdot(H_2O)(D_2O)_{19}$ system but extend to slightly higher energy (by ~50 cm^{-1}). We emphasize that the OH^b_{AAD} envelope has been deconstructed to reveal the heterogeneity of the broad envelope in the Cs^+ system, with two examples presented in Fig. 4. A more complete set of these patterns is presented in Fig. S1, which illustrates how the OH^b_{AAD} broadens and effectively "tunes" through the Fermi resonance with the bend overtone with increasing red-shift. The observed OH^b_{AAD} behavior is not consistent with that calculated (Fig. 5C1), [1,4] however, as there is no observed activity in the region of the higher energy shoulder predicted near 3600 cm^{-1} (labeled β in Fig. 5C). This discrepancy may reflect the fact that at 300 K, the large amplitude motions in the liquid enhance the contributions from more open structures while the cold clusters correspond to the intrinsic behavior of the local minima.

It is more difficult to determine the spectral range of the ADD sites because they do not have a feature common to all of the variations available in the clusters, as do the A and AD sites. Nonetheless, the range in the patterns could be established by probing many frequencies in the 3400-3600 cm^{-1} region where the activity from the ADD site was observed in the previous study of $Cs^+ \cdot (H_2O)_{20}$.[10] Because the cage in $Cs^+ \cdot (H_2O)_{20}$ is the most symmetrical of the PD series, we extended these measurements to the $CH_3NH_3^+$, Li^+, and Na^+ systems. The results are displayed along with the earlier Cs^+ spectra in Fig. 5. Interestingly, all of the activity in the 3400-3600 cm^{-1} range not associated with AD bands appears as a doublet with about same splitting and intensity distribution such that the higher energy member dominates the lower feature by about a factor of two. The doublet splitting and intensity distribution are quite similar in all cases except the Na^+ spectrum (Fig. 5D), which appears broader than those below and above it - an effect likely due to overlapping bands. Note that the range of simulated ADD behavior at the interface (top trace) encompasses that observed experimentally. The fact that these heterogeneous contributions to the spectrum in the 3500 cm^{-1} region occur with similar shapes is surprising and significant. The center frequency of the doublet motif appears to be simply displaced across the predicted region. The issue of whether the ADD doublet arises from the coupling between the OH oscillators when a water molecule is embedded in a network is important, as it involves the question of whether the localized oscillators are degenerate in that binding site (for example using HDO). The observation that the centroid of the doublet motif evolves over 100 cm^{-1}, about the same energy as the splitting between the peaks, while maintaining a similar intensity profile suggests that this splitting is indeed mostly due to the coupling, as opposed to "diagonal disorder" in the local force constants.[2]

III. Qualitative interpretation of trends and theoretical analysis of the network topologies that drive the local OH frequencies of embedded water molecules: Contributions from the second hydration shell and beyond

The general trend in the OH frequencies of the AD and AAD sites is revealed to be $\nu_{AD}^{free} > \nu_{AAD}^{free} > \nu_{AD}^{b} > \nu_{AAD}^{b}$. Qualitatively, we can rationalize this behavior as reflecting the decrease in the effective force constants of both the OH groups when a water molecule accepts a hydrogen bond. When the water molecule has a OH^{free} group, its OH^b frequency is lowered incrementally with the number of H-bonds it accepts. This general trend is also displayed when H_2O binds to metal cations: the presence of positive charge that attracts the electrons on oxygen weakens the bonds to the hydrogen atoms, effectively pushing the positively charged protons away. At the extreme, we note that the OH stretches in H_2O^+ are ~500 cm^{-1} lower than those in H_2O, [37-38] reflecting the connection between the effective force constant and the electron density around the OH bond. Characterization of the H-bonding strength in the context of partial charge transfer has been discussed at length in the context of the isomers formed by the neutral water hexamer.[5, 39] What accounts for the large frequency ranges exhibited by the AAD and AADD sites, given that they all share the same local coordination arrangement? One correlation that accounts for long range interactions is the dependence of the OH^b frequencies on the net local electric field at the bond center.[2, 36] Skinner and Ohno [3, 5] have developed schemes to classify this dependence according to the local network topology. Those maps were generated by exploiting experimental results on the frequencies of the neutral water hexamer to calibrate the methods, and then use these calculations to follow how they are modified in the various isomeric forms. In the scheme reported by Ohno,[3] the index, M, is defined as:

$$M = -d' + a' + d'' - a'' \qquad [1]$$

where d' (0 or 1) and a' (0, 1 or 2) denote the number of additional donor (d') and acceptor (a') H-bonds engaged by the molecule with the OH^b group (gray dashed bonds on the structures in Fig.6A). Similarly, d" (0,1, or 2) and a" (0 or 1) labels the number of additional donor and acceptor H-bonds on the water

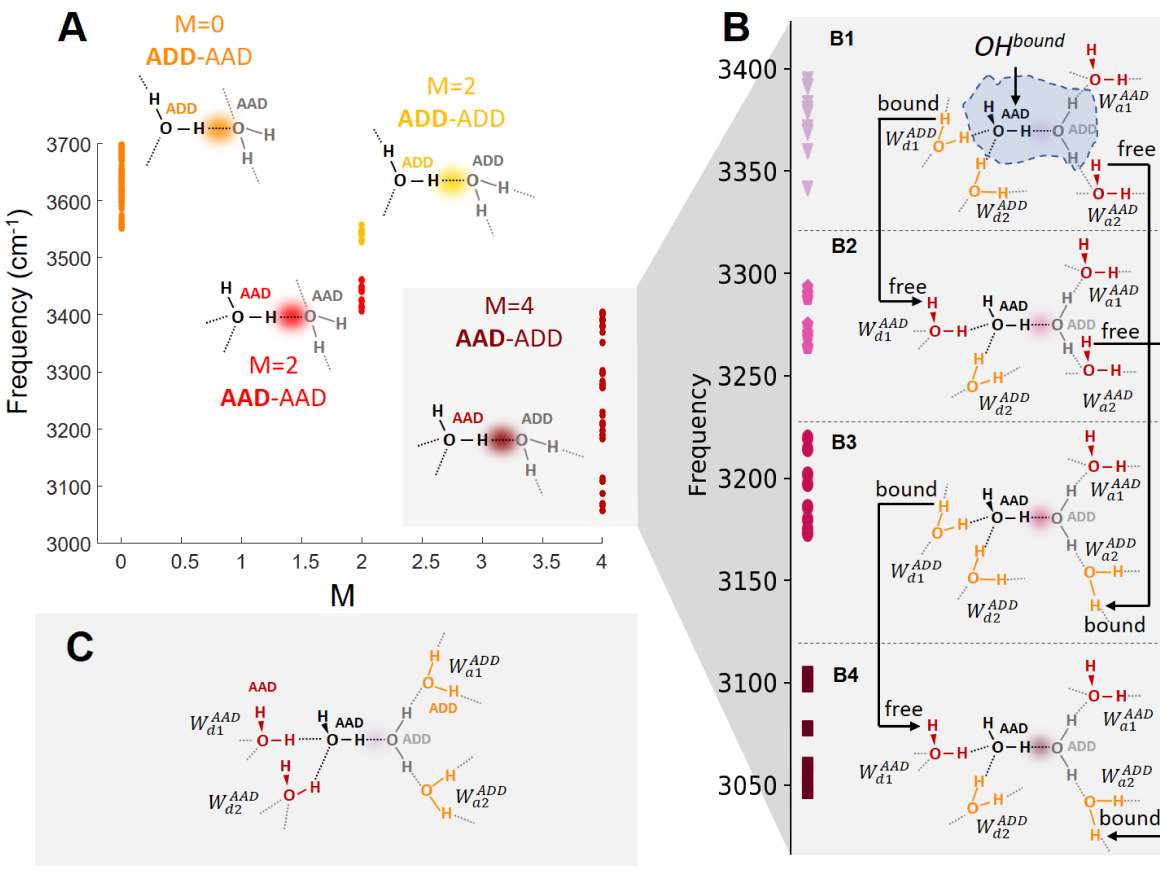

Figure 6. Calculated bound OH frequencies in isomers of the $Cs^+\cdot(H_2O)(D_2O)_{19}$ classified by their hydrogen bond environments. (A) Harmonic frequencies of the bound OH groups plotted against the M index proposed by Ohno.[5] These points are further classified and color coded with an index proposed by Skinner and coworkers, which capture the binding type of both the donor and acceptor water molecules of the H-bond of interest. The schematic structures are shown as water dimers. For example, AAD-ADD corresponds to the case where an OH group on an AAD water molecule donates to an ADD water molecule. The OH oscillators indexed by M=4 (or AAD-ADD) are again further classified in (B) by the binding types of water molecules surrounding the dimer (W_a and W_d). B1 and C represent the environments that yield the weakest and strongest H-bond in the central dimer, respectively. B1-B4 are the structures present in the clusters. The black arrows label the change of exterior water molecule's type from one class to another.

tethered to OH^b. For a specific example, the AAD-ADD pair of water molecules displayed in the lower right of Fig. 6A has the value M = -0+2+2-0 = 4. The points in Fig. 6A are the calculated OH^b frequencies of the all the OH groups in the $Cs^+\cdot(H_2O)(D_2O)_{19}$ PD cage structure, sorted by the M values that encode their H-bonding environments. Indeed, there is a general trend for lower OH^b frequencies with larger M values, but note that the systems identified by M=4 are calculated to vary by ~350 cm^{-1}. Thus, it is evident that variations in the more extended surrounding network must be taken into account to recover the local OH^b behavior.

A useful ansatz that rationalizes the dependence of OH^b frequencies on the surrounding network topology casts a strong H-bond as a frustrated intermolecular proton transfer reaction. [40-41] In that picture, the frequency of the OH group reflects the local endothermicity of this reaction. This is, in turn, determined by how well the extended H-bonding configuration could solvate the incipient H_3O^+ and OH^- ion pair generated by proton transfer.[9] This situation is illustrated in the set of configurations presented in Fig. 6B, which focuses on the AAD site in the specific situation where the donor binds to an ADD molecule, an arrangement that corresponds to M=4 according to Eq. [1]. The key issue is to explore the role played by the site environments occupied by the four molecules solvating the water dimer bound together by the OH^b group (black AAD and gray ADD in dashed box, Fig. 6B1). Two (W_d) donate and two (W_a) accept H-bonds at the four contact points indicated in Fig. 6B1. Both H_3O^+ and OH^- ions adopt threefold hydration shells at the interface and in clusters.[42-44] In the case of H_3O^+, the three molecules in the first hydration shell reside in ADD sites,[24, 42, 45] while those in the first shell around hydroxide adopt the AAD configuration.[46] This is the scenario depicted in Fig. 6C when applied to the pair of water molecules bound by OH^b. By similar reasoning, the arrangement displayed in Fig. 6B1 offers the poorest hydration environment since both W_a and W_d water molecules now reside in sites opposite to those that best solvate the ion pair. The calculated frequencies of the OH^b sites with 6B1 structures are indeed the least red-shifted and form a distinct group near 3375 cm^{-1}. Unfortunately, the favorable 6C arrangement does not occur in the low energy forms of the $Cs^+\cdot(H_2O)_{20}$ PD cage structure. A recent theoretical investigation of the $(H_2O)_{20}$ cluster reported that this arrangement indeed yields the strongest hydrogen bond.[47] Nonetheless, it is instructive to incrementally change the site classes of the four outer water molecules (W_a and W_d in Fig. 6B, gray box) into the more favorable sites, starting from the 6B1 motif. For example, changing a donor water (W_{d1}) from ADD (denoted as W_{d1}^{ADD}) to the AAD (denoted as W_{d1}^{AAD}) orientation with a free OH group yields the 6B2 hydration topology, which indeed identifies a common hydration motif shared by the OH^b oscillators with frequencies around 3275 cm^{-1} (panel 6B2). On the other hand, changing a W_{a2}^{AAD} water to the W_{a2}^{ADD} motif yields the network structure indicated in 6B3, which is the environment common to the OH^b transitions near 3200 cm^{-1}. Note that this group occurs with about twice the shift (relative to the 6B1 class) as those in the 6B2 panel. Interestingly, a similar change in frequency occurs when the one of the W_a waters in the 6B2 structure is switched from AAD to ADD, thus generating the 6B4 arrangement. That topology is common to the group of OH^b transitions near 3075 cm^{-1}, the most red-shifted calculated for this PD structure.

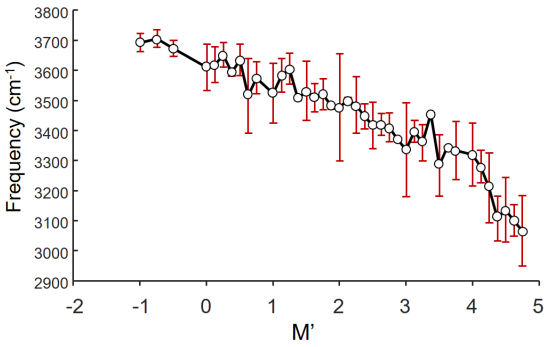

Figure 7. Calculated bound OH frequencies in various water cluster ions sorted by their M' index, defined by Eq. [2]. Harmonic frequency calculation of isomers of the $M^+\cdot(H_2O)(D_2O)_{n-1}$ (M=Li, Na, Cs, ND_4, CD_3NH_3, and n=20) clusters were done at B3LYP/6-31++G** level of theory and basis with the LANL2DZ pseudopotential for Cs. Frequencies were scaled by 0.973.

The trends displayed in Fig. 6B thus elucidate the structural variations experienced by an OH^b group that is most simply described as in an AAD-ADD, M=4 local environment. The calculated frequency groupings in Fig. 6B are distinct because we have focused on the structurally well-defined PD cage in $Cs^+\cdot(H_2O)_{20}$. To introduce a modified index that describes this extended topological-dependence of the OH^b shifts, we first note that the $W_a^{AAD} \rightarrow W_a^{ADD}$ conversion yields about twice the shift as that found for $W_d^{ADD} \rightarrow W_d^{AAD}$. One way to classify the frequencies associated with the four arrangements is

to count the number of hydrogen bonds in W_a and W_d water molecules associated with the solvent structure and account for the fact that changing the bonding to the W_a water molecules induces about twice the shift as do those involving the W_d molecules. A scheme that accounts for the OH^b location for various possible $W_{a,d}$ arrangements with the same M value is provided by M':

$$M' = M + \frac{-d'^{(2)} + a'^{(2)}}{8} + \frac{d''^{(2)} - a''^{(2)}}{4} \qquad [2]$$

where M is the index defined in Eq. [1] and the additional terms capture the shifts induced by the configurations of the $W_{a,d}$ molecules. Specifically, $a'^{(2)}$ and $d'^{(2)}$ are the total number of extra acceptor and donor H-bonds in the W_d water molecules (W_{d1} and W_{d2} in Fig.6B) apart from those to the dimer of interest, whereas $a''^{(2)}$ and $d''^{(2)}$ are the total number of extra acceptor and donor hydrogen bonds in the W_a molecules excluding the ones to the dimer, (W_{a1} and W_{a2} in Fig.6B). The ' and " superscripts denote the donor and acceptor sides of the dimer, which follows the convention established in Eq. [1]. The (2) labels H-bonds as belonging to the second hydration shell. Several example calculations of the M' are provided in Fig. S11. The performance of this index when applied to all of the site configurations in this work is presented in Fig. 7. The M' index thus captures the effect of the sites occupied by water molecules in the first and second hydration shells around a particular OH group.

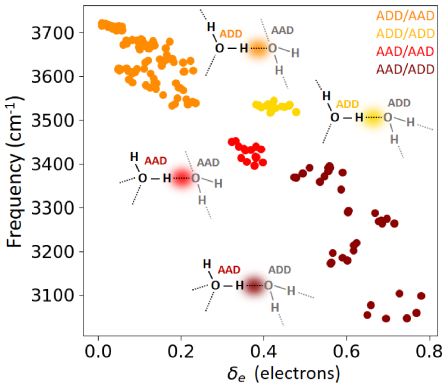

Figure 8. Bound OH frequency dependence on changes in the electron density in the donor OH group and the region along the hydrogen bond. Calculations are carried for the pentagonal dodecahedron cage structure of $Cs^+ \cdot (H_2O)(D_2O)_{19}$. Changes are relative to the densities in the isolated water dimer, held fixed at the geometry of each motif in the cage.

Qualitatively, the M' index reflects the cooperativity and anticooperativity effects caused by the water molecules surrounding the dimer bound by OH^b. In general, when the W_d water molecules accept one or more H-bonds (larger $a'^{(2)}$), the strength of the OH^b bond increases, which is again a statement of cooperativity. The degree of cooperativity depends on the strength of the H-bond between the W_d water molecule and the OH^b. This is most effective when a W_d molecule accepts two H-bonds, and retains the free OH, making its contributions to $d'^{(2)}$ and $a'^{(2)}$ zero and two, respectively.

On the other hand, a W_a water molecule strengthens the H-bond to OH^b the most when it donates two H-bonds (making its contribution to $d''^{(2)} = 2$) and accepts no additional hydrogen bonds (making its contribution to $a''^{(2)} = 0$). The possible ranges of contributions from each second shell water molecule to these parameters are: $d'^{(2)} \in (0,1), a'^{(2)} \in (0,1,2), d''^{(2)} \in (0,1,2), a''^{(2)} \in (0,1)$, and the full ranges of these parameters is twice as large when considering all the second shell water molecules. An interesting observation is that W_a molecules have roughly twice the impact on the H-bond strength than do W_d molecules (reflected as the 1/4 vs. 1/8 factors in Eq. [2]).

The above discussion focused on an empirical connection between the shape of the surrounding network and the OH^b frequency using arguments based on shifts in the electron density. To address the underlying changes in bonding that drive these values, we turn to electronic structure calculations to explore the changes in the electron density in the region of the oxygen atom of the accepting water molecule for various hydrogen bonding geometries depicted in Fig. 6B. Specifically, when a hydrogen

bond is formed, we expect an increase in electron density (δ_{HB}) between the hydrogen atom in the donating water molecule and the oxygen atom in the accepting water molecule along with a decrease in electron density (δ_{OH}) in the region of the OH bond in the donating water molecule. We explored changes to the electron density in these two regions as the strength of the hydrogen bond is tuned through the environments of the donor and acceptor water molecules. We applied this procedure to follow changes in the electronic structure when a water dimer is embedded in a solvation shell of zero to six water molecules (up to three on the open coordination sites on each water). Details are included in the supporting materials. Based on the results for the analysis of these model systems, we characterize changes in the electron density (δ_e) in terms of the differences in the integrated electron density in the hydrogen bond region (δ_{HB}) and along the OH bond that donates into the hydrogen bond (δ_{OH}) when additional water molecules are allowed to form a hydrogen bonding network with the hydrogen bonding pair of water molecules of interest. This analysis is applied to each of the hydrogen bonds in the $Cs^+\cdot(H_2O)_{20}$ pentagonal dodecahedron structure where the other eighteen water molecules provide the additional hydrogen bonding network. Specifically, electron density changes are calculated by taking difference between the electron density in the hydrogen bonding region when the pair of water molecules is incorporated in the $(H_2O)_{20}$ cage relative to the electron density of the isolated dimer. The structures of the donor/acceptor pair of water molecules are the same for both calculations. The effect of the environment on the strength of the hydrogen bond of interest is thus captured by $\delta_e = \delta_{HB} - \delta_{OH}$. Structures where the solvation environment leads to a stronger hydrogen bond (and hence lower frequency) will have $\delta_{HB} > 0$ and $\delta_{OH} < 0$, making δ_e positive.

In Fig. 8, we plot the harmonic OH^b frequencies of all hydrogen-bonded OH stretches in 5 low energy isomers of $Cs^+\cdot(H_2O)(D_2O)_{19}$ as a function of δ_e. The colors are used to differentiate the types of water molecules involved in these hydrogen bonds. As expected from the above discussion, the red shift of the hydrogen-bonded OH bond increases with electron density in the hydrogen-bonding region. We can further explore these effects by identifying the second solvation shell environment for the hydrogen bonds formed between AAD and ADD water molecules (shown in red). The OH bonds with the lowest frequency (and highest electron density in the hydrogen-bonding region) are those for which the acceptor water molecule is donating to an ADD and an AAD water molecule. The higher frequency OH^b groups donate to two AAD water molecules. As discussed above, and seen in Fig. 8, hydrogen bonds to ADD water molecules are stronger (lower frequency) than ones to AAD water molecules when the donor molecule is in the same environment.

IV. Summary

We have isolated the intrinsic spectral signatures of the OH stretching motions on a single water molecule embedded at various sites within the water cage structures that assemble around atomic and molecular cations. This is accomplished using an isotopic labeling scheme in which a single intact H_2O molecule is incorporated into an otherwise perdeuterated cage. The site-specific spectra are then extracted by carrying out two-color, IR-IR photobleaching in an isotopomer-selective mode. The specific patterns recovered with this approach are quite simple, generally consisting of one to three localized absorptions arising from the two correlated fundamentals on the OH groups of the same water molecule. The only complication to this pattern is the appearance of a third band when the red-shifted OH bands fall near the overtone of the HOH intramolecular bending vibration at ~3200 cm^{-1}. Different characteristic patterns are observed for the five binding sites in play at the air-water interface, which differ according to the number of donor and acceptor H-bonds: A, AD, AAD, ADD, and AADD. Although the patterns are preserved in many systems, the frequency ranges over which they appear depend strongly on the site type, with the largest excursions displayed by the sites that yield larger red-shifts (i.e, AAD > AADD > ADD > AD >

A). The simple doublet structure of isolated water arising from the symmetric and antisymmetric OH stretch normal modes is preserved in the ADD sites but with a splitting reduced by about 20%. The AADD sites are the most difficult to characterize because they are embedded in overlapping band structures. Deconvolution yields a single, broadened feature, suggesting suppression of the coupling between the OH group. These results provide a diverse learning set with which to construct extended frequency maps that describe how the IR fundamental of an embedded OH oscillator depends on the topology of the extended water network, and does so in systems that can be treated with accurate theoretical methods.[48-51]

Acknowledgements

MAJ thanks the Chemistry Division of the National Science Foundation for supporting this work under grant CHE-1900119. The IR-IR photofragmentation mass spectrometer crucial for this work was developed under AFOSR DURIP grant FA9550-17-1-0267. ABM thanks the Chemistry division of the National Science Foundation for supporting this work under grant CHE-1856125. Parts of this work were performed using the Ilahie cluster, which was purchased using funds from a MRI grant from the National Science Foundation (CHE-1624430). EM and SSX acknowledge support from the US Department of Energy, Office of Science, Office of Basic Energy Sciences, Division of Chemical Sciences, Geosciences and Biosciences at Pacific Northwest National Laboratory (PNNL). PNNL is a multi-program national laboratory operated for DOE by Battelle. This research also used resources of the National Energy Research Scientific Computing Center, which is supported by the Office of Science of the U.S. Department of Energy under Contract No. DE-AC02-05CH11231

References:

1. Tainter, C. J.; Ni, Y.; Shi, L.; Skinner, J. L. Hydrogen bonding and OH-stretch spectroscopy in water: hexamer (cage), liquid surface, liquid, and ice. *J Phys Chem Lett* **2013,** *4* (1), 12-17.
2. Gruenbaum, S. M.; Tainter, C. J.; Shi, L.; Ni, Y.; Skinner, J. L. Robustness of Frequency, Transition Dipole, and Coupling Maps for Water Vibrational Spectroscopy. *Journal of Chemical Theory and Computation* **2013,** *9* (7), 3109-3117.
3. Ohno, K.; Okimura, M.; Akai, N.; Katsumoto, Y. The effect of cooperative hydrogen bonding on the OH stretching-band shift for water clusters studied by matrix-isolation infrared spectroscopy and density functional theory. *Physical chemistry chemical physics : PCCP* **2005,** *7* (16), 3005-3014.
4. Ni, Y. C.; Skinner, J. L. IR and SFG vibrational spectroscopy of the water bend in the bulk liquid and at the liquid-vapor interface, respectively. *Journal of Chemical Physics* **2015,** *143* (1).
5. Tainter, C. J.; Skinner, J. L. The water hexamer: three-body interactions, structures, energetics, and OH-stretch spectroscopy at finite temperature. *J. Chem. Phys.* **2012,** *137* (10), 104304.
6. Hsieh, C. S.; Okuno, M.; Hunger, J.; Backus, E. H. G.; Nagata, Y.; Bonn, M. Aqueous Heterogeneity at the Air/Water Interface Revealed by 2D-HD-SFG Spectroscopy. *Angewandte Chemie-International Edition* **2014,** *53* (31), 8146-8149.
7. Inoue, K.; Ishiyama, T.; Nihonyanagi, S.; Yamaguchi, S.; Morita, A.; Tahara, T. Efficient Spectral Diffusion at the Air/Water Interface Revealed by Femtosecond Time-Resolved Heterodyne-Detected Vibrational Sum Frequency Generation Spectroscopy. *Journal of Physical Chemistry Letters* **2016,** *7* (10), 1811-1815.
8. Yang, N.; Duong, C. H.; Kelleher, P. J.; Johnson, M. A.; McCoy, A. B. Isolation of site-specific anharmonicities of individual water molecules in the $I^-\cdot(H_2O)_2$ complex using tag-free, isotopomer selective IR-IR double resonance. *Chem. Phys. Lett.* **2017,** *690*, 159-171.
9. Wolk, A. B.; Leavitt, C. M.; Garand, E.; Johnson, M. A. Cryogenic Ion Chemistry and Spectroscopy. *Acc. Chem. Res.* **2014,** *47* (1), 202-210.
10. Yang, N.; Duong, C. H.; Kelleher, P. J.; McCoy, A. B.; Johnson, M. A. Deconstructing Water's Diffuse OH Stretching Vibrational Spectrum With Cold Clusters. *Science* **2019,** *364* (6437), 275-278.
11. Zatula, A. S.; Ryding, M. J.; Andersson, P. U.; Uggerud, E. Proton Mobility and Stability of Water Clusters Containing Alkali Metal Ions. *Int. J. Mass Spec.* **2012,** *330*, 191-199.
12. Ryding, M. J.; Zatula, A. S.; Andersson, P. U.; Uggerud, E. Isotope exchange in reactions between D2O and size-selected ionic water clusters containing pyridine, H+(pyridine)(m)(H2O)(n). *Physical chemistry chemical physics : PCCP* **2011,** *13* (4), 1356-1367.
13. Wolke, C. T.; Fournier, J. A.; Miliordos, E.; Kathmann, S. M.; Xantheas, S. S.; Johnson, M. A. Isotopomer-Selective Spectra of a Single Intact H_2O Molecule in the $Cs^+(D_2O)_5H_2O$ Isotopologue: Going Beyond Pattern Recognition to Harvest the Structural Information Encoded in Vibrational Spectra. *J. Chem. Phys.* **2016,** *144* (7), 074305.
14. Schaefer, J.; Backus, E. H. G.; Nagata, Y.; Bonn, M. Both Inter- and Intramolecular Coupling of O-H Groups Determine the Vibrational Response of the Water/Air Interface. *J Phys Chem Lett* **2016,** *7* (22), 4591-4595.
15. Seki, T.; Sun, S. M.; Zhong, K.; Yu, C. C.; Machel, K.; Dreier, L. B.; Backus, E. H. G.; Bonn, M.; Nagata, Y. Unveiling Heterogeneity of Interfacial Water through the Water Bending Mode. *Journal of Physical Chemistry Letters* **2019,** *10* (21), 6936-6941.
16. Nihonyanagi, S.; Kusaka, R.; Inoue, K.; Adhikari, A.; Yamaguchi, S.; Tahara, T. Accurate determination of complex c(2) spectrum of the air/water interface. *Journal of Chemical Physics* **2015,** *143* (12).
17. Kirov, M. V.; Fanourgakis, G. S.; Xantheas, S. S. Identifying the most stable networks in polyhedral water clusters. *Chemical Physics Letters* **2008,** *461* (4), 180-188.

18. Cooper, R. J.; Chang, T. M.; Williams, E. R. Hydrated Alkali Metal Ions: Spectroscopic Evidence for Clathrates. *J. Phys. Chem. A* **2013,** *117* (30), 6571-6579.
19. Gonzalez, B. S.; Hernandez-Rojas, J.; Wales, D. J. Global minima and energetics of $Li^+(H_2O)_n$, and $Ca^{2+}(H_2O)_n$ clusters for n <= 20. *Chem. Phys. Lett.* **2005,** *412* (1-3), 23-28.
20. Willow, S. Y.; Singh, N. J.; Kim, K. S. NH4+ Resides Inside the Water 20-mer Cage As Opposed to H3O+, Which Resides on the Surface: A First Principles Molecular Dynamics Simulation Study. *Journal of Chemical Theory and Computation* **2011,** *7* (11), 3461-3465.
21. Shin, J.-W.; Hammer, N. I.; Diken, E. G.; Johnson, M. A.; Walters, R. S.; Jaeger, T. D.; Duncan, M. A.; Christie, R. A.; Jordan, K. D. Infrared signature of structures associated with the $H^+\cdot(H_2O)_n$ (n = 6 to 27) clusters. *Science* **2004,** *304* (5674), 1137-1140.
22. Skinner, J. L.; Pieniazek, P. A.; Gruenbaum, S. M. Vibrational Spectroscopy of Water at Interfaces. *Accounts Chem Res* **2012,** *45* (1), 93-100.
23. Fournier, J. A.; Wolke, C. T.; Johnson, C. J.; Johnson, M. A.; Heine, N.; Gewinner, S.; Schollkopf, W.; Esser, T. K.; Fagiani, M. R.; Knorke, H.; Asmis, K. R. Site-specific vibrational spectral signatures of water molecules in the magic $H_3O^+\cdot(H_2O)_{20}$ and $Cs^+\cdot(H_2O)_{20}$ clusters. *Proc. Natl. Acad. Sci.* **2014,** *111* (51), 18132-18137.
24. Fournier, J. A.; Johnson, C. J.; Wolke, C. T.; Weddle, G. H.; Wolk, A. B.; Johnson, M. A. Vibrational spectral signature of the proton defect in the three-dimensional $H^+\cdot(H_2O)_{21}$ cluster. *Science* **2014,** *344* (6187), 1009-1012.
25. Stachl, C. N.; Williams, E. R. Effects of Temperature on $Cs^+(H_2O)_{20}$ Clathrate Structure. *Journal of Physical Chemistry Letters* **2020,** *11*, 6127-6132.
26. Xantheas, S. S. Low-lying energy isomers and global minima of aqueous nanoclusters: Structures and spectroscopic features of the pentagonal dodecahedron $(H_2O)_{20}$ and $H_3O^+(H_2O)_{20}$. *Can J Chem Eng* **2012,** *90* (4), 843-851.
27. Robertson, W. H.; Weddle, G. H.; Kelley, J. A.; Johnson, M. A. Solvation of the $Cl^-\cdot H_2O$ Complex in CCl_4 Clusters: The Effect of Solvent-Mediated Charge Redistribution on the Ionic H-Bond. *J. Phys. Chem. A* **2002,** *106*, 1205-1209.
28. McCoy, A. B. The role of electrical anharmonicity in the association band in the water spectrum. *J. Phys. Chem. B* **2014,** *118* (28), 8286-8294.
29. McCoy, A. B.; Guasco, T. L.; Leavitt, C. M.; Olesen, S. G.; Johnson, M. A. Vibrational manifestations of strong non-Condon effects in the $H_3O^+\cdot X_3$ (X = Ar, N_2, CH_4, H_2O) complexes: a possible explanation for the intensity in the "association band'' in the vibrational spectrum of water. *Phys. Chem. Chem. Phys.* **2012,** *14* (20), 7205-7214.
30. Roscioli, J. R.; Diken, E. G.; Johnson, M. A.; Horvath, S.; McCoy, A. B. Prying apart a water molecule with anionic H-bonding: a comparative spectroscopic study of the $X^-\cdot H_2O$ (X = OH, O, F, Cl, and Br) binary complexes in the 600-3800 cm^{-1} region. *J. Phys. Chem. A* **2006,** *110* (15), 4943-4952.
31. Yang, N.; Duong, C. H.; Kelleher, P. J.; Johnson, M. A. Capturing intrinsic site-dependent spectral signatures and lifetimes of isolated OH oscillators in extended water networks. *Nat. Chem.* **2020,** *12*, 159-164.
32. Li, F.; Skinner, J. L. Infrared and Raman line shapes for ice Ih. II. H2O and D2O. *Journal of Chemical Physics* **2010,** *133* (24).
33. Shimanouchi, T. *Tables of Molecular Vibrational Frequencies Consolidated Volume I, National Bureau of Standards*. 1972; p 1-160.
34. Hermansson, K. Electric-field effects on the OH vibrational frequency and infrared absorption intensity for water. *J. Chem. Phys.* **1993,** *99*, 861-868.
35. Carnegie, P. D.; Bandyopadhyay, B.; Duncan, M. A. Infrared Spectroscopy of Mn+(H2O) and Mn2+(H2O) via Argon Complex Predissociation. *Journal of Physical Chemistry A* **2011,** *115* (26), 7602-7609.

36. Kebede, G. G.; Mitev, P. D.; Briels, W. J.; Hermansson, K. Red-shifting and blue-shifting OH groups on metal oxide surfaces - towards a unified picture. *Physical chemistry chemical physics : PCCP* **2018,** *20* (18), 12678-12687.
37. Roth, D.; Dopfer, O.; Maier, J. P. Intermolecular potential energy surface of the proton-bound H2O+-He dimer: Ab initio calculations and IR spectra of the O-H stretch vibrations. *Physical chemistry chemical physics : PCCP* **2001,** *3* (12), 2400-2410.
38. Huet, T. R.; Pursell, C. J.; Ho, W. C.; Dinelli, B. M.; Oka, T. Infrared-Spectroscopy and Equilibrium Structure of H2o+(X)over-Tilde2b1). *Journal of Chemical Physics* **1992,** *97* (9), 5977-5987.
39. Guevara-Vela, J. M.; Romero-Montalvo, E.; Gomez, V. A. M.; Chavez-Calvillo, R.; Garcia-Revilla, M.; Francisco, E.; Pendas, A. M.; Rocha-Rinza, T. Hydrogen Bond Cooperativity and Anticooperativity Within the Water Hexamer. *Phys. Chem. Chem. Phys.* **2016,** *18* (29), 19557-19566.
40. Craig, S. M.; Menges, F. S.; Duong, C. H.; Denton, J. K.; Madison, L. R.; McCoy, A. B.; Johnson, M. A. Hidden Role of Intermolecular Proton Transfer in the Anomalously Diffuse Vibrational Spectrum of a Trapped Hydronium Ion. *Proc. Natl. Acad. Sci. USA* **2017,** *114* (24), E4706-E4713.
41. Duong, C. H.; Yang, N.; Johnson, M. A.; DiRisio, R. J.; McCoy, A. B.; Yu, Q.; Bowman, J. M. Disentangling the Complex Vibrational Mechanics of the Protonated Water Trimer by Rational Control of Its Hydrogen Bonds. *J. Phys. Chem. A* **2019,** *123* (37), 7965-7972.
42. Fournier, J. A.; Wolke, C. T.; Johnson, M. A.; Odbadrakh, T. T.; Jordan, K. D.; Kathmann, S. M.; Xantheas, S. S. Snapshots of proton accommodation at a microscopic water surface: understanding the vibrational spectral signatures of the charge defect in cryogenically cooled $H^+ \cdot (H_2O)_{n=2-28}$ clusters. *J. Phys. Chem. A* **2015,** *119* (36), 9425-9440.
43. Robertson, W. H.; Diken, E. G.; Price, E. A.; Shin, J. W.; Johnson, M. A. Spectroscopic determination of the OH- solvation shell in the OH-center dot(H2O)(n) clusters. *Science* **2003,** *299* (5611), 1367-1372.
44. Mundy, C. J.; Kuo, I. F. W.; Tuckerman, M. E.; Lee, H. S.; Tobias, D. J. Hydroxide Anion at the Air-water Interface. *Chemical Physics Letters* **2009,** *481* (1-3), 2-8.
45. Fournier, J. A.; Wolke, C. T.; Johnson, C. J.; Johnson, M. A.; Heine, N.; Gewinner, S.; Schollkopf, W.; Esser, T. K.; Fagiani, M. R.; Knorke, H.; Asmis, K. R. Site-Specific Vibrational Spectral Signatures of Water Molecules in the Magic $H_3O^+(H_2O)_{20}$ and $Cs^+(H_2O)_{20}$ Clusters. *Proc. Natl. Acad. Sci.* **2014,** *111* (51), 18132-18137.
46. Bankura, A.; Chandra, A. Hydration structure and dynamics of a hydroxide ion in water clusters of varying size and temperature: Quantum chemical and ab initio molecular dynamics studies. *Chem Phys* **2012,** *400*, 154-164.
47. Alexei A. Kananenka, J. L. S. Unusually strong hydrogen bond cooperativity in particular $(H_2O)_{20}$ clusters. *Physical chemistry chemical physics : PCCP* **2020,** *Advance Article*.
48. Paesani, F.; Voth, G. A. The Properties of Water: Insights from Quantum Simulations. *J. Phys. Chem. B* **2009,** *113* (17), 5702-5719.
49. Reddy, S. K.; Moberg, D. R.; Straight, S. C.; Paesani, F. Temperature-dependent vibrational spectra and structure of liquid water from classical and quantum simulations with the MB-pol potential energy function. *Journal of Chemical Physics* **2017,** *147* (24).
50. Riera, M.; Gotz, A. W.; Paesani, F. The i-TTM model for ab initio-based ion-water interaction potentials. II. Alkali metal ion-water potential energy functions. *Physical chemistry chemical physics : PCCP* **2016,** *18* (44), 30334-30343.
51. Ceriotti, M.; Fang, W.; Kusalik, P. G.; McKenzie, R. H.; Michaelides, A.; Morales, M. A.; Markland, T. E. Nuclear Quantum Effects in Water and Aqueous Systems: Experiment, Theory, and Current Challenges. *Chem. Rev.* **2016,** *116* (13), 7529-7550.